

# Magnetic actuation of paramagnetic liquids for optical beam steering in high-speed optical wireless communications

Mithilesh K. Mane<sup>1,2</sup>, Amjad Ali<sup>1,2,3</sup>, Riffat Tehseen<sup>1</sup>, Arfan Mahmood<sup>1</sup>, and Jing Xu (徐敬)<sup>1,2,3\*</sup>

<sup>1</sup>Optical Communication Laboratory, Ocean College, Zhejiang University, Zhoushan 316021, China

<sup>2</sup>Hainan Institute of Zhejiang University, Sanya 572025, China

<sup>3</sup>Donghai Laboratory, Zhoushan 316021, China

\*Corresponding author: [jxu-optics@zju.edu.cn](mailto:jxu-optics@zju.edu.cn)

Received November 4, 2024 | Accepted December 25, 2024 | Posted Online May 20, 2025

This study examines paramagnetic liquids for optical beam steering in optical wireless communication (OWC) systems. By employing magnetic actuation, effective optical beam control was achieved for both free-space optics (FSO) and underwater wireless optical communication (UWOC). Experimental findings revealed that dysprosium nitrate provided the highest beam steering angles of  $5.99^\circ$  in the  $\pm X$  direction and  $5.73^\circ$  in the  $\pm Y$  direction. Additionally, power loss analysis indicated minimal absorption and scattering for dysprosium nitrate and gadolinium nitrate. The system achieved high-speed data rates of 2.1 Gbps for FSO and 1.9 Gbps for UWOC systems, showcasing the promise of this technology.

**Keywords:** optical beam steering; paramagnetic liquid; optical wireless communication; free-space optics; underwater wireless optical communication.

**DOI:** [10.3788/COL202523.060603](https://doi.org/10.3788/COL202523.060603)

## 1. Introduction

Optical wireless communication (OWC) has gained importance due to its high data rate, high security, and strong immunity to electromagnetic interference, making it ideal for both free-space optics (FSO) and underwater wireless optical communication (UWOC) systems<sup>[1-3]</sup>. Optical beam steering (OBS), a crucial component of OWC, is divided into mechanical and non-mechanical techniques. Mechanical techniques<sup>[4]</sup>, such as micro-electromechanical systems, rotating prisms, rotating mirrors, polygons, and digital micro-mirror devices (DMDs), rely on moving parts but are limited in speed, precision, reliability, and size. However, non-mechanical techniques<sup>[5,6]</sup>, such as optical phased arrays (OPAs), liquid-crystal (LC) micro-lenses, acousto-optic deflectors (AODs), polarized gratings, metasurfaces, and liquid prisms (LPs) offer enhanced performance by eliminating moving parts, making them a critical focus in OWC research<sup>[6,7]</sup>.

For instance, LC micro-lenses using the electro-optic effect achieved a maximum diagonal steering angle of  $\pm 3.42^\circ$ <sup>[8]</sup>, while metasurfaces enabled continuous beam steering up to  $70^\circ$  by regulating phase, amplitude, and polarization of light<sup>[9]</sup>. OPAs, through phase control of optical elements, demonstrated a steering range of  $17^\circ$  and data rates of 10 Gbit/s<sup>[10]</sup>. Electrowetting on dielectric (EWOD) achieved a  $14.82^\circ$  angle

with data rates of 1.9 Gbps (FSO) and 1.7 Gbps (UWOC) by adjusting liquid-liquid interface curvature under an electric field<sup>[11]</sup>. Beam steering with an  $18^\circ$  field of view and a data rate of 1.8 GHz was enabled by the AOD, facilitating high-speed frequency-domain LiDAR imaging<sup>[12]</sup>. A longitudinal scanning angle of  $32.10^\circ$  and a beam steering efficiency of  $0.55^\circ/\text{nm}$  were achieved through the utilization of polarization multiplexing and etching depth optimization<sup>[13]</sup>. Collectively, these non-mechanical techniques represent significant advancements in OWC, offering robust, agile, and miniaturized systems.

Magnetic fields have been widely studied for manipulating liquid droplets. Various droplet manipulation techniques have been developed under the influence of magnetic fields, such as droplet generation, deformation, transportation, sorting, coalescence, splitting, and levitation<sup>[14]</sup>. Advances such as reconfigurable magnetic liquid metal robots allow simultaneous manipulation of multiple droplets<sup>[15]</sup>, while soft magnetic carpets dynamically control droplets by switching surface states between sticky and slippery under a magnetic field<sup>[16]</sup>. Salts such as manganese chloride ( $\text{MnCl}_2$ )<sup>[17]</sup>, manganese sulfate ( $\text{MnSO}_4$ )<sup>[18]</sup>, manganese nitrate [ $\text{Mn}(\text{NO}_3)_2$ ]<sup>[19]</sup>, dysprosium nitrate [ $\text{Dy}(\text{NO}_3)_3$ ]<sup>[20]</sup>, and gadolinium nitrate [ $\text{Gd}(\text{NO}_3)_3$ ]<sup>[21]</sup> exhibit paramagnetic properties due to their unpaired electrons.  $\text{Gd}^{3+}$  with seven and  $\text{Dy}^{3+}$  with five unpaired electrons in their

respective subshells contribute to strong magnetic responses under a magnetic field due to their high-spin  $4f$  configurations. Similarly, the  $\text{Mn}^{2+}$  ion contains five unpaired electrons in the 3D subshell, which align with an external magnetic field, causing these chemicals to exhibit paramagnetism. These unpaired electrons generate magnetic dipoles that align with an external magnetic field, enhancing their magnetic susceptibility.

Magnetic actuation utilizes external magnetic fields to control motion in materials like paramagnetic liquids, which exhibit positive magnetic susceptibility ( $\chi$ ) when exposed to a magnetic field, becoming weakly magnetized. Unlike ferromagnetic materials, paramagnetic liquids do not retain magnetization without an applied field. The induced magnetization ( $M$ ) interacts with the magnetic field ( $H$ ), generating a force that moves or deforms the liquid, driving it toward regions of higher magnetic field strength<sup>[22]</sup>. This equation encapsulates the core principle of magnetic actuation in paramagnetic materials:

$$M = \chi_m H. \quad (1)$$

Recent studies in paramagnetic materials, which exhibit magnetic properties when exposed to magnetic fields, represent significant breakthroughs in scientific and industrial applications. To the best of our knowledge, this study is the first to experimentally demonstrate OBS using paramagnetic salts in the OWC domain under varied conditions. It showcases the potential of field forces like magnetic actuation to achieve beam steering without internal mechanical components. Such magnetic field-based technologies offer promise for precise control and rapid response time, advancing compact, energy-efficient OWC systems for FSO and UWOC.

## 2. Materials and Methods

### 2.1. Paramagnetic materials

In this study, manganese chloride ( $\text{MnCl}_2$ ), manganese sulfate ( $\text{MnSO}_4$ ), and manganese nitrate [ $\text{Mn}(\text{NO}_3)_2$ ] were utilized for their strong paramagnetic properties due to the  $\text{Mn}^{2+}$  ions, which contain five unpaired electrons in the 3D orbital. These chemicals are effective for OBS when exposed to a magnetic field. Similarly, gadolinium nitrate [ $\text{Gd}(\text{NO}_3)_3$ ], and dysprosium nitrate [ $\text{Dy}(\text{NO}_3)_3$ ] were selected for their  $\text{Dy}^{3+}$  and  $\text{Gd}^{3+}$  ions, which have multiple unpaired electrons in the  $4f$  orbital, further enhancing paramagnetism and influencing beam directionality.

Each chemical was prepared as an aqueous solution and subjected to controlled magnetic fields to evaluate their effectiveness in OBS, focusing on the role of paramagnetic materials in advanced optical technologies. Stock solutions of manganese chloride, manganese nitrate, manganese sulfate, dysprosium nitrate, and gadolinium nitrate were prepared by dissolving the respective chemicals in deionized water (5 ml) until a saturated solution was achieved. The concentrations of these stock solutions are given in Table 1, which ensures consistency across experiments. Subsequently, another set of dysprosium nitrate solutions was prepared in 5 ml of deionized water to examine

Table 1. The Concentrations of These Stock Solutions.

Sr no.	Paramagnetic salt	Deionized water (ml)	Added chemical wt. (g)	Ratio
1	$\text{MnCl}_2$	5	3.8283	1:0.766
2	$\text{MnSO}_4$	5	2.6400	1:0.528
3	$\text{Mn}(\text{NO}_3)_2$	5	6.2974	1:1.259
4	$\text{Gd}(\text{NO}_3)_3$	5	5.3365	1:1.120
5	$\text{Dy}(\text{NO}_3)_3$	5	5.5986	1:1.067

Table 2. The Concentrations of Dysprosium Nitrate Solutions.

Sr no.	Deionized water (ml)	Added chemical wt. (g)	Ratio
1	5	1.3997	1:0.2799
2	5	2.7993	1:0.5597
3	5	4.1990	1:0.8398
4	5	5.5986	1:1.1200

the effect of varying concentrations on the beam steering angle, as shown in Table 2.

### 2.2. Hydrophobic materials

In this study, we utilized polytetrafluoroethylene (PTFE), a synthetic fluoropolymer of tetrafluoroethylene, specifically AF Teflon (6% 1601x, DuPont), which is chosen for its exceptional hydrophobic characteristics and high optical transparency. Additionally, it provides a low surface energy coating, which improves the durability of devices by minimizing defect formation.

### 2.3. Fabrication process

A cylindrical tube of quartz glass with an inner diameter of 10 mm, a wall thickness of 1 mm, and a height of 10 mm was used as the base for fabricating the paramagnetic LP, and a 2 mm flat glass sheet was secured at the bottom using a UV-curable adhesive. The LP was first cleaned with acetone and dried before being coated with a 6% AF Teflon solution to create a thin hydrophobic layer using the dip-coating method, ensuring uniform coating. The Teflon coating was cured by initially heating the prism at 115°C for 16 h, then increasing the temperature to 140°C for 3 h, and finally heating it at 170°C for 10 min. The LP was then filled with concentrated stock solutions, as outlined in Table 1 and Table 2, along with ethyl acetate. To finalize the sealed prism assembly, a second glass slide was attached to the top of the prism. We chose ethyl acetate as the second liquid because it does not mix with water due to its difference in

polarity. Additionally, ethyl acetate has a lower density ( $0.902\text{ g/cm}^3$ ) compared to water ( $1.0\text{ g/cm}^3$ ), allowing it to form a distinct top layer when combined. The absence of precipitation in the sealed glass prisms and stock solutions after prolonged storage suggests that the paramagnetic liquids maintain physical and chemical stability over time. A neodymium magnet with a strength of  $1.2\text{ T}$  was used for experimental analysis.

### 3. Experimental Setup

Figure 1(a) shows the schematic diagram of the experimental setup for OBS using a paramagnetic liquid prism (PMLP) for an OWC system, comprising a transmitter, an optical channel, and a receiver. Figure 1(b) presents photographs and detailed configurations of a transmitter, a 2 m water tank, and a receiver setup for FSO and UWOC links.

The experimental setup features a commercially available  $520\text{ nm}$  single-mode fiber-pigtailed laser diode (LD) (LP520-SF17, Thorlabs), chosen for its narrow beam profile and high modulation bandwidth. The LD is mounted in an LDM9LP LD/TEC mount (Thorlabs) and controlled by an LD/TEC driver (ITC4020, Thorlabs). The system's transmission performance was evaluated using the non-return-to-zero on-off keying (NRZ-OOK) modulation scheme, via a bit error rate tester (BERT, MP2100B), which generated a pseudo-random binary sequence with a pattern length of to modulate the LD. In this proof-of-concept experiment, the OBS was controlled using a PMLP, which was actuated by a permanent magnet due to the lack of a proper electromagnet. The frequency response was characterized using a network analyzer (Hewlett Packard 8753D). At the receiver, the optical signal was initially collimated by a  $72\text{ mm}$  diameter spherical lens before passing through an optical variable attenuator, followed by a  $1\text{ GHz}$  silicon avalanche photodiode (APD210, Thorlabs). Output power measurements were conducted using a power meter (PM100D, Thorlabs).

## 4. Results and Discussion

### 4.1. Beam steering

Figures 2(a)–2(e) show the effect of an external magnetic field on various paramagnetic chemicals, including manganese chloride, manganese sulfate, manganese nitrate, gadolinium nitrate, and dysprosium nitrate. The lateral displacement of the optical beam spot was recorded using a graph paper on a linear scale. To convert this linear displacement into an angular value, the trigonometric relation  $\theta = \tan^{-1}\left(\frac{D_1}{D_2}\right)$  was applied. Here,  $D_1$  represents the horizontal displacement of the beam spot, while  $D_2$ , fixed at  $23\text{ cm}$ , is the distance between the PMLP and the graph paper.

The experiment aimed to determine which paramagnetic chemical exhibited the highest OBS angle when exposed to an external magnetic field. The beam steering angle was then determined along the  $\pm XY$  axes. Dysprosium nitrate demonstrated the most significant beam steering, with a maximum displacement of  $\pm 1.2\text{ cm}$  along both the  $X$  and  $Y$  axes. Manganese nitrate also showed a considerable OBS angle with values reaching up to  $\pm 1.1\text{ cm}$ . Other chemicals, such as manganese chloride, manganese sulfate, and gadolinium nitrate, exhibited moderate beam steering displacements. The observed beam steering can be attributed to the strong magnetic actuation of these paramagnetic chemicals when subjected to an external magnetic field, where the unpaired electrons in these materials align with the magnetic field, causing directional displacement. This alignment enhances their responses to the magnetic field, facilitating precise control of the beam's optical path. The observed optical beam deflection angles are listed in Table 3 for respective paramagnetic chemicals.

To convert the angle  $\theta$  and the distance  $r$  (cm) from the center location into  $XY$  coordinates, we can use the trigonometric functions:  $x = r \cdot \cos \theta$  and  $y = r \cdot \sin \theta$ , where  $\theta$  represents the angle in degrees, while the cosine and sine functions transform the polar coordinates into Cartesian coordinates. Figures 2(f)–2(i) show the impact of the magnetic field on different

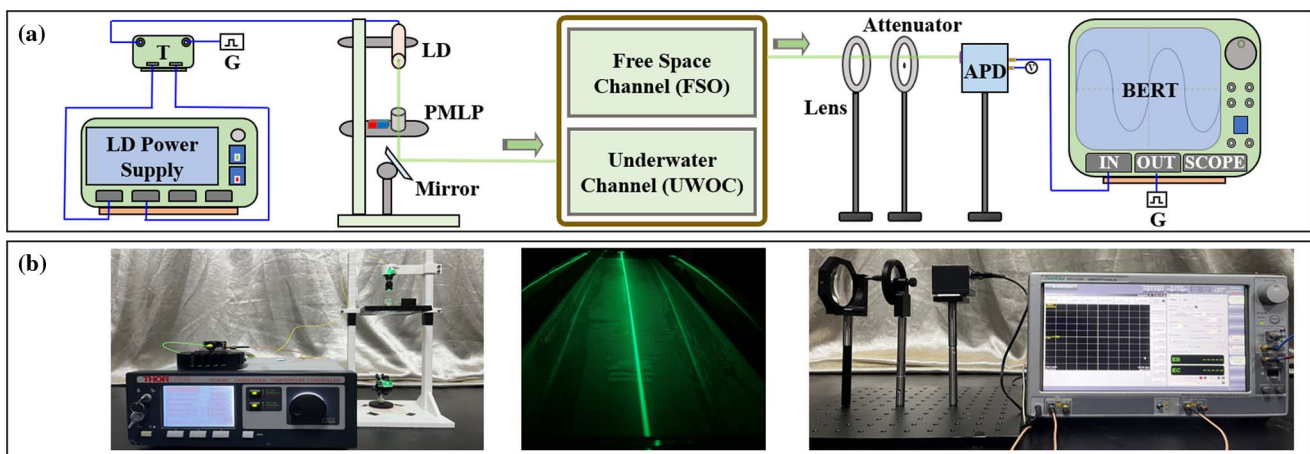
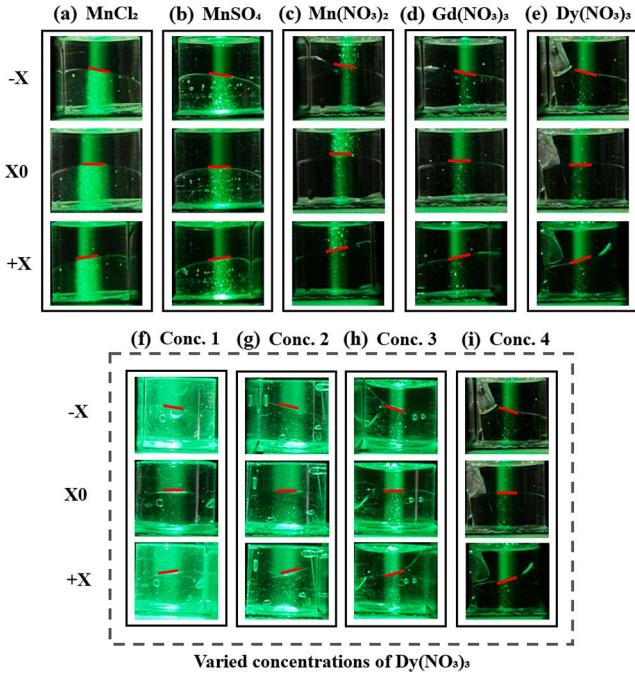


Fig. 1. (a) The schematic diagram of the experimental setup for OBS using a paramagnetic liquid prism. (b) Photographs of a transmitter, a 2 m water tank, and a receiver for FSO and UWOC links.



**Fig. 2.** Front-facing images depict the behavior of the paramagnetic liquid in response to an external magnetic field. (a)–(e) Effect of an external magnetic field on various paramagnetic chemicals. (f)–(i) Impact of the magnetic field on different concentrations of dysprosium nitrate. The label X0 represents the liquid’s orientation in the absence of any magnetic field. In contrast, +X and –X illustrate the liquid’s orientation when subjected to a magnetic field, with +X showing steering toward the right side of the prism and –X showing steering toward the left.

**Table 3.** Observed OBS Along the ±X and ±Y Axes for Various Paramagnetic Chemicals When Exposed to an External Magnetic Field.

Sr no.	Paramagnetic chemical	–X	+X	–Y	+Y
1	MnCl <sub>2</sub>	–0.6	0.5	–0.5	0.6
2	MnSO <sub>4</sub>	–0.5	0.4	–0.5	0.5
3	Mn(NO <sub>3</sub> ) <sub>2</sub>	–1.0	1.1	–1.1	1.0
4	Gd(NO <sub>3</sub> ) <sub>3</sub>	–0.6	0.6	–0.5	0.6
5	Dy(NO <sub>3</sub> ) <sub>3</sub>	–1.2	1.1	–1.2	1.1

concentrations of dysprosium nitrate, where increasing the concentration results in a progressively intensified yellowish tint.

The observed beam steering angles in Fig. 3(a) for varying concentrations of dysprosium nitrate under the influence of an external magnetic field show a clear increase of beam displacement with higher concentrations. Figure 3(a) shows a decrease in optical intensity versus the concentration of Dy(NO<sub>3</sub>)<sub>3</sub>, as indicated in Table 2.

As shown in Fig. 3(b), MnSO<sub>4</sub> and MnCl<sub>2</sub> cause the highest power loss due to absorption and scattering, making them less

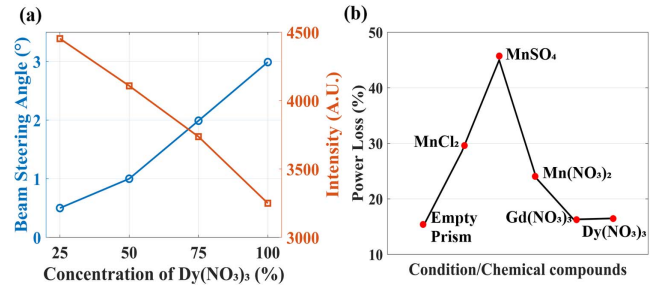


**Fig. 3.** (a) Beam steering angles and received optical intensities for different concentrations of dysprosium nitrate. (b) Percentage of power loss in the empty prism and paramagnetic chemicals compared to the direct output power of the LD.

suitable for optical applications. In contrast, Gd(NO<sub>3</sub>)<sub>3</sub> and Dy(NO<sub>3</sub>)<sub>3</sub> exhibit minimal power loss, making them ideal for optical transmission. The results suggest that power loss is strongly linked to the inherent optical properties of the chemicals, with rare-Earth nitrates being the most transparent.

At the lowest concentration, a beam steering angle of ~0.5° was observed, indicating moderate interaction between the magnetic field and the paramagnetic material. The steering effect became more noticeable as the concentration increased; the subsequent concentration resulted in a steering angle of ~1°, followed by ~2° at a higher concentration. The highest concentration exhibited the most significant beam steering, achieving an ~3° angle. This progressive increase suggests that higher concentrations of dysprosium nitrate enhance the material’s paramagnetic properties, leading to a stronger alignment of magnetic dipoles with the external field and, thus, greater control over the optical beam’s trajectory.

Based on the results in Table 3, dysprosium nitrate exhibited the highest beam steering in an external magnetic field. Therefore, it was selected for further experimental analysis in the optical communication link. Figure 4(a) shows the maximum displacement of the optical beam spot observed at various XY coordinates along a 360° path in a 2D plane, as listed in Table 4. Using dysprosium nitrate, OWC links for both FSO and UWOC systems were established at distinct beam steering

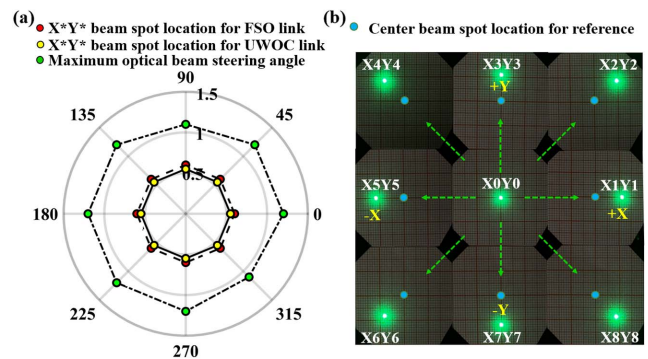


**Fig. 4.** (a) A schematic illustration of the optical beam spot on the XY plane, showing the beam spot configurations used in optical communication measurements. (b) Optical beam spot measurements along the X and Y axes.

**Table 4.** Beam Spot Location for the Measurements of the OWC Links (Cartesian Coordinates).

XY denotation	Maximum beam steering observed	XY location (FSO)	XY location (UWOC)
X0Y0	0.0, 0.0	0.0, 0.0	0.0, 0.0
X1Y1	1.2, 0.0	0.6, 0.0	0.5, 0.0
X2Y2	0.85, 0.85	0.42, 0.42	0.39, 0.39
X3Y3	0.0, 1.1	0.0, 0.6	0.0, 0.5
X4Y4	-0.85, 0.85	-0.42, 0.42	-0.39, 0.39
X5Y5	-1.2, 0.0	-0.6, 0.0	-0.5, 0.0
X6Y6	-0.85, -0.85	-0.42, -0.42	-0.39, -0.39
X7Y7	0.0, -1.2	0.0, -0.6	0.0, -0.5
X8Y8	0.78, -0.78	0.42, -0.42	0.39, -0.39

angles. Figure 4(b) presents an actual photograph of the LD beam spot on a graph paper. A maximum beam displacement was noted at positions X2Y2, X5Y5, and X7Y7, with a beam steering angle as high as 2.99° measured in free space. The FSO and UWOC link measurements were carried out at the distinct locations on a 2D plane as listed in Table 4. The paramagnetic properties of dysprosium nitrate, influenced by an external magnetic field, contributed to the controlled steering of the optical beam, showing promising results in both communication mediums. The proposed paramagnetic liquid-based OBS system facilitates a total beam steering angle of 5.98° along the ±X axes and 5.73° along the ±Y axes. The system demonstrated a resolution of 0.125°, measured using a 16-bit Dhyana 400BSI sCMOS camera, with a precision of 0.068°. These results highlight its capability to accurately and efficiently steer optical beams, showcasing potential for practical applications.

**4.2. Optical wireless communication**

The P-I and V-I output characteristics of the LD are presented in the inset of Fig. 5. Figure 5 illustrates the frequency response of the LD-APD back-to-back system without the PMLP, along with the PMLP-based FSO communication system and the PMLP-based UWOC system. The crosstalk ratio was calculated to be 0.41%, and the insertion loss was found to be 2.27 dB, indicating efficient optical power transmission with minimal interference.

The frequency response analysis indicates that the maximum 3 dB bandwidths for the LD, FSO, and UWOC links stabilize at 1039, 1022, and 1014 MHz, respectively, at 70 mA. Furthermore, the optical transmission link capacity of the proposed LP-based beam steering system is investigated using NRZ-OOK modulation over a transmission distance of 2 m in both free-space and underwater environments.

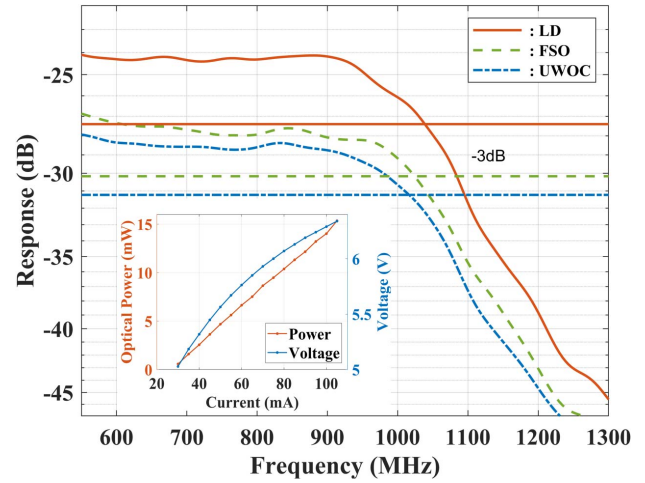


**Fig. 5.** Frequency responses of the LD-APD back-to-back system, LP-based FSO communication system, and LP-based UWOC system. The inset presents the P-I and V-I curves of the 520 nm pigtail LD.

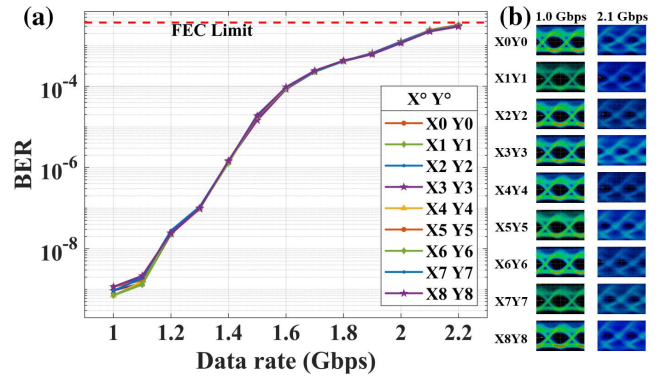


**Fig. 6.** (a) Measured BER of the FSO communication link in the 2D plane, and (b) corresponding eye diagrams at various XY locations for data rates of 1.0 and 2.1 Gbps.

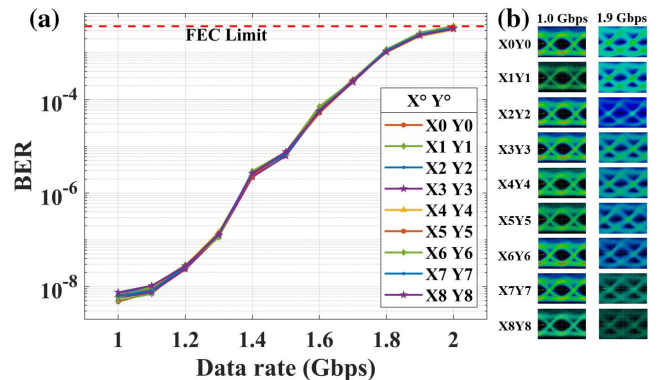


**Fig. 7.** (a) Measured BER of the UWOC link in the 2D plane, and (b) corresponding eye diagrams at various XY locations for data rates of 1.0 and 1.9 Gbps.

**Table 5.** Previously Reported Studies on Various Non-Mechanical Beam-Steering Techniques.

Ref.	Technique	Angle	Data rate	Remark
[10]	OPA	17°	10 Gbps	OBS and OWC
[8]	LC micro-lens	±3.42°	NA	OBS
[13]	Polarized grating	32.1°	NA	OBS
[12]	APD	18°	1.8 Gbps	LiDAR
[9]	Metasurface	70°	NA	
[11]	EWOD	14.82°	1.9 Gbps	OBS and OWC
This study	Magnetic actuation	5.98° along the ±X axes and 5.73° along the ±Y axes	2.1 Gbps (FSO) and 1.9 Gbps (UWOC)	OBS and OWC

Figures 6 and 7 illustrate the FSO and UWOC links using PMLP in a 2D plane, respectively, with beam steering angles outlined in Table 4. Figure 6 shows the data rate and bit error rate (BER) for each ±XY location of the FSO communication link, and the corresponding eye diagrams for data rates of 1.0 and 2.1 Gbps. Similarly, Fig. 7 shows the data rate and BER for each ±XY location of the UWOC link, and the corresponding eye diagrams for data rates of 1.0 and 1.9 Gbps. The measured BER adheres to the standard forward error correction (FEC) threshold of  $3.8 \times 10^{-3}$ . The proposed paramagnetic liquid-based LP beam steering system can support high-speed optical data transmission links up to 2.1 Gbps for the FSO system and 1.9 Gbps for the UWOC system. Table 5 summarizes previously reported studies on various non-mechanical beam-steering techniques.

## 5. Conclusion

This study introduces an innovative approach for OBS in OWC systems using paramagnetic liquids, with a focus on dysprosium nitrate for its strong paramagnetic properties. Experimental results demonstrated that dysprosium nitrate achieved the highest beam displacement ( $\pm 1.2$  cm) and the maximum steering angle of 5.98° along the ±X axes and 5.73° along the ±Y axes, outperforming other paramagnetic chemicals. The system demonstrated a resolution of 0.125° and a precision of 0.068°. Power loss analysis confirms that rare-Earth nitrates, especially dysprosium and gadolinium, are ideal for optical transmission. Crosstalk was measured at a low value of 0.41%, with an insertion loss of 2.27 dB, highlighting minimal interference between channels. The system supports high data rates up to 2.1 Gbps (FSO) and 1.9 Gbps (UWOC) with acceptable BERs, showing the potential of paramagnetic liquid-based beam steering for flexible OWC systems in next-generation communication technologies.

## Acknowledgements

This work was supported by the Key Research and Development Program of Hainan Province (No. ZDYF2023GXJS016)

and the National Key Research and Development Program of China (No. 2022YFC2808200).

## References

- J. Xu, "Underwater wireless optical communication: why, what, and how?" *Chin. Opt. Lett.* **17**, 100007 (2019).
- E. E. Elsayed, M. R. Hayal, I. Nurhidayat, *et al.*, "Coding techniques for diversity enhancement of dense wavelength division multiplexing MIMO-FSO fault protection protocols systems over atmospheric turbulence channels," *IET Optoelectron.* **18**, 11 (2024).
- E. E. Elsayed, "Atmospheric turbulence mitigation of MIMO-RF/FSO DWDM communication systems using advanced diversity multiplexing with hybrid N-SM/OMI M-ary spatial pulse-position modulation schemes," *Opt. Commun.* **562**, 130558 (2024).
- P. F. McManamon, "Review of lidar: a historic, yet emerging, sensor technology with rich phenomenology," *Opt. Eng.* **51**, 060901 (2012).
- P. F. McManamon, "A review of non mechanical beam steering options," in *LEOS 2008-21st Annual Meeting of the IEEE Lasers and Electro-Optics Society* (2008), p. 575.
- Y. Cheng, J. Cao, and Q. Hao, "Optical beam steering using liquid-based devices," *Opt. Lasers Eng.* **146**, 106700 (2021).
- P. F. McManamon and A. Ataei, "Progress and opportunities in the development of nonmechanical beam steering for electro-optical systems," *Opt. Eng.* **58**, 120901 (2019).
- M. G. de Blas, J. P. García, S. V. Andreu, *et al.*, "High resolution 2D beam steerer made from cascaded 1D liquid crystal phase gratings," *Sci. Rep.* **12**, 5145 (2022).
- P. Thureja, G. K. Shirmanesh, K. T. Fountaine, *et al.*, "Array-level inverse design of beam steering active metasurfaces," *ACS Nano* **14**, 15042 (2020).
- C.-W. Chow, Y.-C. Chang, S.-I. Kuo, *et al.*, "Actively controllable beam steering optical wireless communication (OWC) using integrated optical phased array (OPA)," *J. Lightwave Technol.* **41**, 1122 (2022).
- M. K. Mane, A. Ali, R. Tehseen, *et al.*, "Non-mechanical beam steering for high-speed optical wireless communications via electrowetting on dielectric," *Opt. Express* **32**, 28792 (2024).
- B. Li, Q. Lin, and M. Li, "Frequency-angular resolving LiDAR using chip-scale acousto-optic beam steering," *Nature* **620**, 316 (2023).
- T. Fu, X. Yan, X. Zhang, *et al.*, "Inverse-designed polarization multiplexing non-uniformly distributed gratings for one-dimensional beam steering," *Opt. Express* **31**, 6051 (2023).
- G.-P. Zhu, Q.-Y. Wang, Z.-K. Ma, *et al.*, "Droplet manipulation under a magnetic field: a review," *Biosensors* **12**, 156 (2022).
- Y. Zhang, S. Jiang, Y. Hu, *et al.*, "Reconfigurable magnetic liquid metal robot for high-performance droplet manipulation," *Nano Lett.* **22**, 2923 (2022).
- A. F. Demirörs, S. Aykut, S. Ganzboom, *et al.*, "Programmable droplet manipulation and wetting with soft magnetic carpets," *Proc. Natl. Acad. Sci.* **118**, e2111291118 (2021).

17. G. DeFotis, R. Wiese, and C. Scherrer, "MnCl<sub>2</sub> · H<sub>2</sub>O: a quasi-one-dimensional Heisenberg antiferromagnet," *J. Appl. Phys.* **67**, 5857 (1990).
18. Y. Allain, J. Krebs, and J. De Gunzbourg, "Magnetic study of the manganous sulfates MnSO<sub>4</sub> and MnSO<sub>4</sub> · H<sub>2</sub>O," *J. Appl. Phys.* **39**, 1124 (1968).
19. A. C. Yadav, P. R. Tiwari, R. P. Singh, *et al.*, "Synthesis and characterization of manganese doped zinc ferrite for its structural and magnetic properties," *Iranian J. Sci.* **48**, 269 (2024).
20. M. Guo, Y. Wang, J. Wu, *et al.*, "Structures and magnetic properties of dysprosium complexes: the effect of crystallization temperature," *Dalton Trans.* **46**, 564 (2017).
21. S. Laurent, C. Henoumont, D. Stanicki, *et al.*, "Paramagnetic gadolinium complexes," in *MRI Contrast Agents: From Molecules to Particles* (Springer, 2017), p. 23.
22. W. D. Callister, Jr. and D. G. Rethwisch, *Materials Science and Engineering: an Introduction* (John Wiley & sons, 2020).